Complex Formation of Trimethylaluminum and Trimethylgallium with Ammonia: Evidence for a Hydrogen-Bonded Adduct

George T. Wang* and J. Randall Creighton

Sandia National Laboratories, Sandia National Laboratories, P.O. Box 5800, MS-0601, Albuquerque, New Mexico 87185

Received: July 26, 2005; In Final Form: November 16, 2005

We have investigated the formation of gas-phase adducts of trimethylaluminum and trimethylgallium with ammonia using room-temperature Fourier transform infrared experiments and density functional theory calculations. Our results indicate for the first time that, at higher partial pressures, a product distinct from the well-known $(CH_3)_3M{:}NH_3$ adduct grows in for both M = Al and M = Ga. Comparison of the experimental and calculated IR spectra, along with calculations of the energetics, indicates that this second product is the result of hydrogen bonding of a second NH_3 molecule to the $(CH_3)_3M{:}NH_3$ adduct and can be written as $(CH_3)_3M{:}NH_3{\cdots}NH_3$. The binding energy of this hydrogen-bonded adduct is calculated to be 26.8 kcal/mol for M = Al and 18.4 kcal/mol for M = Ga and is lower in energy (more stable) relative to the 1:1 $(CH_3)_3M{:}NH_3$ adduct by 7.2 kcal/mol for M = Al and 6.6 kcal/mol for M = Ga. In contrast, an alternative complex involving the formation of two separate M−N donor−acceptor bonds, which is written as $H_3N{:}(CH_3)_3M{:}NH_3$, is calculated to be lower in energy relative to $(CH_3)_3M{:}NH_3$ by only 0.1 kcal/mol for M = Al and 0.2 kcal/mol for M = Ga and is not observed experimentally. These results show that hydrogen bonding plays an important role in the interaction of ammonia with metal organic precursors involving Al, Ga, and In, under typical metal organic chemical vapor deposition AlGaInN growth conditions.

Introduction

The group III nitrides, including GaN and AlGaInN alloys, are an important class of semiconductors currently used in a number of optoelectronic applications, including light emitting diodes and lasers. Currently, metal organic chemical vapor deposition (MOCVD), typically employing the precursors trimethylaluminum (TMAl), trimethylgallium (TMGa), trimethylindium (TMIn), and ammonia (NH_3), is the dominant technique used to deposit device-quality III-nitride materials. Unfortunately, gas-phase reactions between these organometallic precursors and ammonia can have parasitic effects that make control and reproducibility of the growth process difficult.[1−9]

Upon mixing with ammonia, it is widely known that TMAl, TMGa, and TMIn will undergo the reversible formation of a donor−acceptor complex via attack of the lone-pair electrons of NH_3 at the electron-deficient metal atom of the organometallic precursor, as shown in

$$M(CH_3)_3 + NH_3 \leftrightarrow (CH_3)_3M{:}NH_3 \qquad M = Al, Ga, In \quad (1)$$

Formation of the $(CH_3)_3M{:}NH_3$ adduct is of interest because it represents the first step from which further parasitic chemical reactions may take place and thus has been widely studied.[4,9−24] Creighton et al. previously showed that these parasitic reactions can even lead to the formation of gas-phase nanoparticles.[25,26]

In this paper, we have taken a combined experimental and theoretical approach to elucidate the nature of the adduct formation between ammonia and trimethylaluminum or trimethylgallium. We report here the gas-phase infrared spectra of the complexes of TMAl and TMGa with NH_3 at room temperature, along with density functional theory quantum chemical calculations of the energetics and infrared frequencies. We have also isolated experimentally and identified, for the first time, the formation of an additional, distinct "2:1" adduct involving a single TMAl or TMGa molecule and two NH_3 molecules, which increases in relative concentration as the partial pressures are increased. We can thus expand reaction 1 as

$$M(CH_3)_3 + 2NH_3 \leftrightarrow (CH_3)_3M{:}NH_3 + NH_3 \leftrightarrow (CH_3)_3M{:}(NH_3)_2 \qquad M = Al, Ga, In \quad (2)$$

Previous theoretical work has considered the complexation of a second NH_3 molecule with the metal atom of the $(CH_3)_3M{:}NH_3$ adduct, forming a doubly coordinated $H_3N{:}(CH_3)_3M{:}NH_3$ adduct with two M−N bonds.[19,21] A reasonable assumption thus may be to assign the identity of the experimentally observed 2:1 adduct as this doubly coordinated $H_3N{:}(CH_3)_3M{:}NH_3$ adduct. However, we present here for the first time experimental and theoretical results that indicate that this adduct instead involves the hydrogen bonding of a second NH_3 molecule to the $(CH_3)_3M{:}NH_3$ adduct, rather than coordination to the metal atom.

Theoretical and Experimental Methods

Main-group chemistry has been widely studied using density functional theory (DFT) methods. DFT calculations using the B3LYP hybrid functional[27] were employed in this study to examine the chemistry between TMAl and TMGa with NH_3. The Gaussian 03 software package was used for all the calculations.[28] Geometry optimizations were carried out without symmetry constraints using the 6-31G(d) basis set to locate the stationary points on the potential energy surface. Species

* Corresponding author. E-mail: gtwang@sandia.gov.

10.1021/jp054133o CCC: $33.50
Published on Web 12/24/2005

involving hydrogen bonding were reoptimized using a larger 6-311++G(d,p) basis set incorporating diffuse and polarization functions on the hydrogen atoms. Single-point energy and frequency calculations using the 6-311++G(d,p) basis set were performed for each stationary point to obtain the zero-point energies, thermal corrections, and infrared frequencies. The calculated stationary points on the potential energy surface were verified by analysis of the normal modes as minima by the absence of imaginary frequencies. All energies reported in this paper have been zero-point-corrected. Enthalpies were calculated at 298 K and 1 atm of pressure. Calculated frequencies were scaled using factors primarily determined using a least-squares fitting analysis comparing the calculated versus experimental spectra.[29] The scaling factors ranged from 0.95 to 0.97. Calculated infrared spectra were synthesized using the calculated frequencies and intensities, assuming Gaussian line shapes with a 26 cm^{-1} full width at half-maximum (fwhm). Peak assignments were made via visualization of the normal modes from the Gaussian log file.

Gas-phase infrared spectroscopy was performed with a Mattson RS-1 FTIR spectrometer at 2 cm^{-1} resolution. A heatable long path length gas cell was mounted in the sample compartment of the instrument. Briefly, the IR beam enters and exits through a single KCl window (6 mm thickness) and is folded once with a Au-coated spherical mirror (r = 40.6 cm), giving an internal path length of ~80 cm. This intermediate value of path length gives a reasonable absorbance for the organometallic precursors and adducts without producing an excessive absorbance from the gas-phase NH_3 (which is 200−800× higher in concentration). In all spectra shown for $(CH_3)_3M + NH_3$ mixtures, the very large NH_3 spectrum has been removed for clarity. The gas cell was connected in parallel with our research MOCVD reactor and operated at flow rates and pressures in the same nominal range used for AlGaInN deposition. Gases were mixed before injection into the cell, with concentrations kept below the onset of adduct condensation.[30] A long internal gas inlet tube allowed the gases to preheat before they were fully introduced into the cell.

The total pressure was varied from 50 to 300 Torr, with a total flow rate of 6500 cm^3(STP) min^{-1}. For this flow rate, at 300 K and 100 Torr total pressure, the mean residence time in the cell is 3.54 s (internal volume = 3.2 L). Hydrogen was used as the carrier gas. The ammonia flow rate was fixed at 1000 cm^3(STP) min^{-1}, giving $P(NH_3)$ = 7.7 Torr at the 50 Torr total pressure condition. TMAl and TMGa were delivered using a standard bubbler configuration to give P(TMAl−monomer) = 11.7 mTorr [31] and P(TMGa) = 31.4 mTorr [32] at the 50 Torr total pressure condition. We assume that TMAl is 100% dimerized at the bubbler conditions and give flow rates and partial pressures on a TMAl monomer basis. The partial pressure of the reactant scales with total pressure, so at 300 Torr the values are 6-fold greater than the 50 Torr values given above. The flow rates of TMAl and TMGa in this study were set at 1.52 and 4.08 cm^3(STP) min^{-1}, respectively. All spectra were taken at room temperature (24 °C).

Theoretical Results

The optimized geometries of the adducts of TMAl and NH_3 considered in this paper are shown in Figure 1. The calculated geometries of the complexes of TMGa and NH_3 have virtually identical conformations to those of TMAl and NH_3 and hence are not separately shown. Selected geometric parameters of interest are also shown in Figure 1 for both TMAl and TMGa. Calculated binding energies and changes in enthalpies of all products relative to the reactants are given in Table 1.

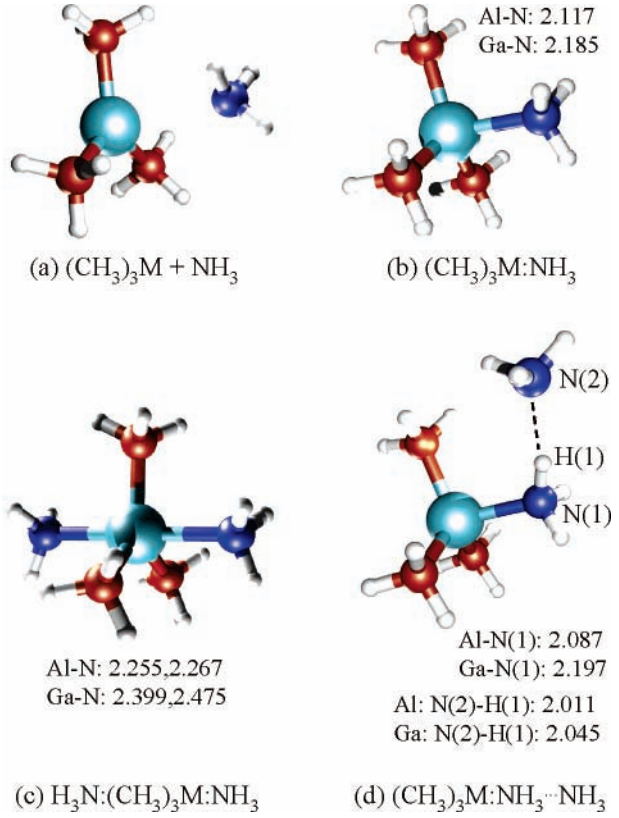

Figure 1. Optimized geometries of (a) unassociated $(CH_3)_3M$ and NH_3, (b) 1:1 $(CH_3)_3M:NH_3$, (c) 2:1 $H_3N:(CH_3)_3M:NH_3$, and (d) 2:1 hydrogen-bonded $(CH_3)_3M:NH_3\cdots NH_3$.

The optimized geometry of the 1:1 $(CH_3)_3Al:NH_3$ adduct is shown in Figure 1b. Complex formation is energetically favorable, with a calculated binding energy ($-\Delta E_{ZPE}$) of 19.6 kcal/mol and an enthalpy change of −20.4 kcal/mol relative to the reactants. This compares to previous calculations of ΔE = −20.2 to −25.9 kcal/mol [18,19,23] and ΔH = −27 kcal/mol [21] for $(CH_3)_3Al:NH_3$. The structure of $(CH_3)_3Al:NH_3$ has been previously discussed in detail, and the calculated Al−N bond length of 2.117 Å for $(CH_3)_3Al:NH_3$ agrees well with previous calculations.[12,18] For $(CH_3)_3Ga:NH_3$, we calculate a binding energy of 11.8 kcal/mol and a change in enthalpy of −12.6 kcal/mol. These values are slightly below previous calculations of ΔE = −14.4 to −20 kcal/mol [19,23,33] and ΔH = −15.9 to −20.5 kcal/mol.[21,22,24,33] Previous experimental estimates of ΔH range from −15.2 to −16.3 kcal/mol.[33,34] The calculated Ga−N bond length of 2.185 Å is similar in magnitude to previous calculations[22−24] and an electron diffraction study which reported a Ga−N bond length of 2.161 Å.[14]

It is also possible for a second NH_3 molecule to attack the metal atom of the 1:1 $(CH_3)_3M:NH_3$ complex to form a second M−N donor−acceptor bond, as shown in Figure 1c. We previously reported the observation in the magnesocene ($MgCp_2$ or $Mg(C_5H_5)_2$) + NH_3 system of an analogous adduct also involving two donor−acceptor bonds, i.e., $H_3N:MgCp_2:NH_3$, at higher partial pressures.[35] The 2:1 $H_3N:(CH_3)_3M:NH_3$ complex is calculated (relative to the reactants $(CH_3)_3M + 2NH_3$) to have a binding energy of 19.7 kcal/mol and ΔH of −21.1 kcal/mol where M = Al and a binding energy of 12.0 kcal/mol and ΔH of − 12.9 kcal/mol where M = Ga. The stabilization energy added by the second M−N donor−acceptor bond relative to the 1:1 $(CH_3)_3M:NH_3$ adduct is only 0.1 kcal/mol for M = Al and 0.2 kcal/mol for M = Ga. Thus, it is seen that the formation of the 2:1 $H_3N:(CH_3)_3M:NH_3$ complex is only

TABLE 1: Relative Energies and Enthalpies (kcal/mol) of the Calculated Species Shown in Figure 1, Calculated at the B3LYP/6-311++G(d,p) Level of Theory

	M = Al			M = Ga		
	ΔE	ΔE_{ZPE}	ΔH	ΔE	ΔE_{ZPE}	ΔH
$(CH_3)_3M + 2NH_3$	0	0	0	0	0	0
$(CH_3)_3M{:}NH_3 + NH_3$	−22.5	−19.6	−20.4	−14.6	−11.8	−12.6
$H_3N{:}(CH_3)_3M{:}NH_3$	−24.8	−19.7	−21.1	−16.3	−12.0	−12.9
$(CH_3)_3M{:}NH_3\cdots NH_3$	−31.4	−26.8	−27.6	−22.7	−18.4	−19.0

energetically favorable over the 1:1 complex by a minimal amount. The calculated average length of the two Al−N bonds in $H_3N{:}(CH_3)_3Al{:}NH_3$ is 2.261 Å, a substantial increase from the calculated Al−N bond length of 2.087 Å in the 1:1 $(CH_3)_3Al{:}NH_3$ adduct. This increase in bond length indicates a significant decrease in the strength of the Al−N donor−acceptor bond upon formation of the second Al−N donor−acceptor bond. A similar phenomenon is observed for $H_3N{:}(CH_3)_3Ga{:}NH_3$, where the calculated average length of the two Ga−N bonds is 2.437 Å, versus 2.185 Å in the 1:1 $(CH_3)_3Ga{:}NH_3$ adduct. Compared to these results, Nakamura et al. calculated that formation of the 2:1 $H_3N{:}(CH_3)_3M{:}NH_3$ adduct results in a greater (but still weak) stabilization energy of 5.7 kcal/mol for M = Al and 3.1 kcal/mol for M = Ga, relative to the $(CH_3)_3M{:}NH_3$ adduct.[19] Simka et al. calculated the formation of $H_3N{:}(CH_3)_3Ga{:}NH_3$ as being 5.2 kcal/mol more energetically favorable compared to $(CH_3)_3Ga{:}NH_3$.[21]

We also consider here for the first time an alternative complex resulting from hydrogen bonding of the nitrogen atom of a second NH_3 molecule to a hydrogen atom of the NH_3 molecule in the 1:1 $(CH_3)_3M{:}NH_3$ adduct, as shown in Figure 1d. The binding energy of this 2:1 hydrogen-bonded adduct, which we write as $(CH_3)_3M{:}NH_3\cdots NH_3$, is calculated to be 26.8 kcal/mol for M = Al and 18.4 kcal/mol for M = Ga. This formation of this hydrogen bond represents a stabilization energy relative to the 1:1 $(CH_3)_3M{:}NH_3$ adduct of 7.2 kcal/mol for M = Al and 6.6 kcal/mol for M = Ga. In comparison, recent theoretical studies of the hydrogen-bonded ammonia dimer $(NH_3)_2$ have calculated a weaker interaction energy of 1.6−3.8 kcal/mol.[36−39] The stronger interaction in the 2:1 hydrogen-bonded $(CH_3)_3M{:}NH_3\cdots NH_3$ adduct is likely due to the greater electron deficiency of the NH_3 molecule (compared to unassociated NH_3) involved in the donor−acceptor bond with TMAl or TMGa.

Significantly, the theoretical calculations thus indicate that formation of the 2:1 hydrogen-bonded $(CH_3)_3M{:}NH_3\cdots NH_3$ adduct is energetically favored over the 2:1 $H_3N{:}(CH_3)_3M{:}NH_3$ complex by a substantial amount. The calculated Al−N and Ga−N bond lengths of 2.087 and 2.197 Å, respectively, in the hydrogen-bonded $(CH_3)_3M{:}NH_3\cdots NH_3$ adduct are almost unchanged from their values in the 1:1 $(CH_3)_3M{:}NH_3$ adduct, indicating that this donor−acceptor bond is not significantly perturbed upon formation of the hydrogen bond. The N···H hydrogen bond length is calculated to be 2.011 Å for $(CH_3)_3Al{:}NH_3\cdots NH_3$ and 2.045 Å for $(CH_3)_3Ga{:}NH_3\cdots NH_3$.

Experimental Results

Trimethylaluminum + NH_3. We have collected the room-temperature gas-phase infrared spectra of the products resulting from mixing TMAl or TMGa with NH_3. Figure 2b shows the room-temperature IR spectrum of TMAl mixed with NH_3 at a total pressure of 50 Torr. The spectrum contains no discernible contribution from uncomplexed, gas-phase TMAl (not shown), and thus the TMAl is considered to be completely associated with NH_3. The spectrum at 50 Torr is largely similar to the spectrum reported previously at 99 °C at 100 Torr by Creighton et al.,[26] which was identified as the $(CH_3)_3Al{:}NH_3$ adduct in part by comparison with earlier condensed-phase spectra of $(CH_3)_3Al{:}NH_3$.[10,11,18] When the pressure is increased to 300 Torr, the infrared spectrum (Figure 2c) shows the disproportionately strong growth of several peaks (marked by vertical lines) which were very weak or not visible in the spectrum taken at 50 Torr. This indicates an increase in the relative concentration of a second distinct product as the pressure is increased, where the growth peaks represent the new modes of the second product. This observation is consistent with reaction 2, whereby increasing the pressure will shift the equilibrium from the 1:1 $(CH_3)_3Al{:}NH_3$ adduct toward a 2:1 $(CH_3)_3Al{:}(NH_3)_2$ adduct involving a second NH_3 molecule, according to Le Chatelier's principle. Examination of the calculated spectrum of the 1:1 $(CH_3)_3Al{:}NH_3$ adduct, shown in Figure 2a, shows an excellent fit to the spectrum at 50 Torr (Figure 2b). Moreover, the calculated 1:1 $(CH_3)_3Al{:}NH_3$ spectrum (Figure 2a) fails to predict the two growth peaks in the 300 Torr data (Figure 2c) at 1053 and 3126 cm^{-1} that can be associated with the 2:1 adduct. The results thus show that, at 50 Torr, the product mixture at room temperature consists primarily of the 1:1 $(CH_3)_3Al{:}NH_3$ adduct and that, at 300 Torr, the product mixture shifts toward a greater fraction of the 2:1 $(CH_3)_3Al{:}(NH_3)_2$ adduct.

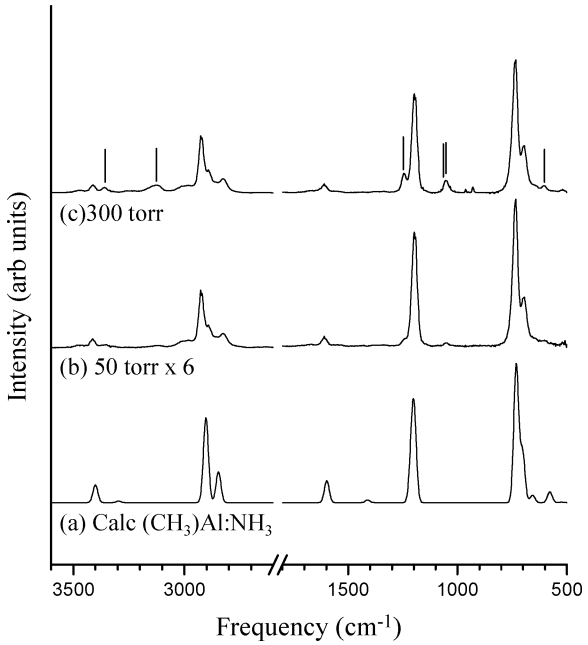

Figure 2. (a) Calculated IR spectrum of $(CH_3)_3Al{:}NH_3$ (frequency scale factor = 0.96), (b) experimental IR spectrum of $(CH_3)_3Al{:}NH_3 + NH_3$ at 50 Torr, and (c) $(CH_3)_3Al{:}NH_3 + NH_3$ at 300 Torr.

To spectrally isolate and identify the 2:1 adduct, the contribution of the 1:1 $(CH_3)_3Al{:}NH_3$ complex was removed from the 300 Torr spectrum via subtraction of a multiple (5.2) of the 50 Torr spectrum. The multiple is less than the simple ratio of the pressures (300/50 = 6) because at 300 Torr there is proportionately less 1:1 $(CH_3)_3Al{:}NH_3$ adduct than at 50 Torr, due to an increase of the 2:1 adduct. The resulting difference spectrum,

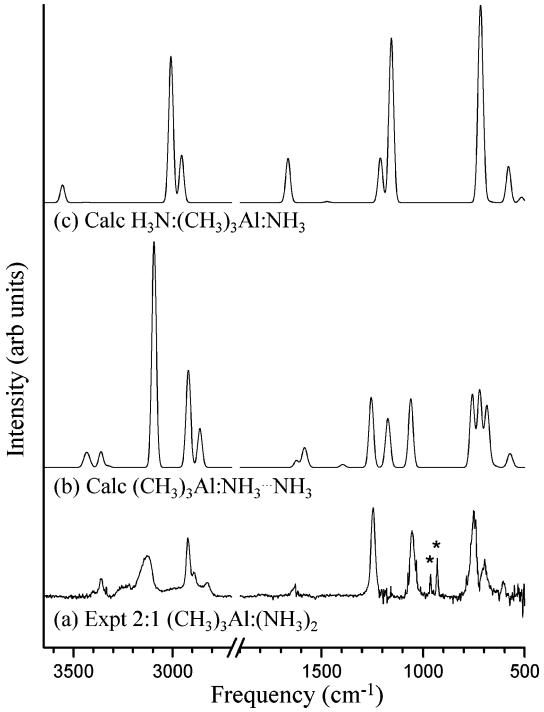

Figure 3. (a) Isolated experimental difference IR spectrum of 2:1 $(CH_3)_3Al$:$(NH_3)_2$ and (b) calculated IR spectrum of hydrogen-bonded $(CH_3)_3Al$:NH_3···NH_3 (frequency scale factor = 0.96 for ν(N−H) and ν(C−H) modes, 0.95 all other modes), and (c) calculated IR spectrum of H_3N:$(CH_3)_3Al$:NH_3 (frequency scale factor = 0.96 for ν(N−H) and ν(C−H) modes, 0.97 all other modes). Asterisks represent residual NH_3 peaks.

which represents the 2:1 adduct, is shown in Figure 3a. To determine the identity of the 2:1 complex, we plotted the calculated spectrum of the hydrogen-bonded $(CH_3)_3Al$:NH_3··· NH_3 adduct, shown in Figure 3b, along with that of the H_3N: $(CH_3)_3Al$:NH_3 complex, shown in Figure 3c. It is seen that the spectrum of the hydrogen-bonded adduct matches the experimental 2:1 adduct spectrum quite accurately and correctly predicts the experimental peaks at 1054, 1245, 3126, and 3361 cm^{-1}, which are modes that increase in relative intensity as the pressure is increased and can thus be uniquely assigned to the 2:1 adduct. In contrast, the calculated spectrum of the H_3N: $(CH_3)_3Al$:NH_3 complex is a much poorer fit overall and notably fails to predict the 2:1 adduct experimental peaks at 1054, 1245, 3126, and 3361 cm^{-1}.

On the basis of this analysis, we identify the 2:1 $(CH_3)_3Al$: $(NH_3)_2$ adduct, which increases in relative concentration as the pressure is increased, as the hydrogen-bonded $(CH_3)_3Al$: NH_3···NH_3 adduct. This assignment is consistent with the theoretical calculations of the energetics, which predicts that the hydrogen-bonded $(CH_3)_3Al$:NH_3···NH_3 adduct is lower in energy (more stable) by 7.1 kcal/mol relative to the 2:1 H_3N: $(CH_3)_3Al$:NH_3 complex. The observed experimental frequencies are listed in Table 2, along with selected mode assignments taken from the corresponding calculated hydrogen-bonded $(CH_3)_3Al$:NH_3···NH_3 frequencies.

Trimethylgallium + NH_3. The results for TMGa + NH_3 are very similar to those of TMAl + NH_3. Figure 4b shows the room-temperature IR spectrum of TMGa mixed with NH_3 at a total pressure of 50 Torr. The spectrum at 50 Torr is largely identical to that reported by Creighton et al.[26] at 53 °C and 100 Torr, which was identified as the $(CH_3)_3Ga$:NH_3 adduct. The spectrum is also in good agreement with previous reports of the gas-phase spectrum of $(CH_3)_3Ga$:NH_3.[13−15] The calculated

TABLE 2: Experimental and Selected Calculated Frequencies (cm^{-1}) and Relative Intensities (arb units) for the Hydrogen-Bonded $(CH_3)_3Al$:$N^{(1)}H_3$···$N^{(2)}H_3$ Adduct

exp	calc[a]	I	assignment
	380	3	ν(Al−N)
	483	7	ν_s(Al−C_3)
	567	16	ν_{as}(Al−C_3)
606	578	21	ν_{as}(Al−C_3)
698	688	130	$\delta(CH_3)_{rock}$
	722	184	$\delta(N^{(1)}H_3)_{rock}$ + $\delta(CH_3)_{rock}$
751	758	174	$\delta(N^{(1)}H_3)_{rock}$ + $\delta(CH_3)_{rock}$
1054	1060	164	$\delta_s(N^{(2)}H_3)$ umbrella
	1168	50	$\delta_s(CH_3)$
	1174	51	$\delta_s(CH_3)$
1245	1254	168	$\delta_s(N^{(1)}H_3)$ umbrella
1627	1623	16	$\delta_{as}(N^{(1)}H_3)$
2825	2860	43	$\nu(CH_3)$
2885	2863	46	$\nu(CH_3)$
2892	2865	5	$\nu(CH_3)$
	2914	36	$\nu(CH_3)$
2919	2918	37	$\nu(CH_3)$
	2919	62	$\nu(CH_3)$
2924	2924	12	$\nu(CH_3)$
	2925	99	$\nu(CH_3)$
3126	3094	539	$\nu_s(N^{(1)}H_3)$
	3327	4	$\nu_s(N^{(2)}H_3)$
3361	3362	37	$\nu_{as}(N^{(1)}H_3)$
	3434	20.8	$\nu_{as}(N^{(2)}H_3)$

[a] ν(C−H) and ν(N−H) modes scaled by 0.96; all other modes scaled by 0.95.

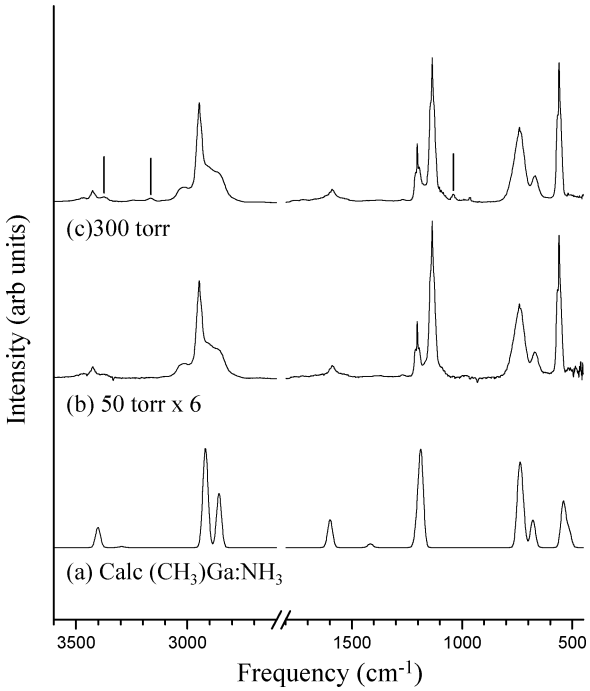

Figure 4. (a) Calculated IR spectrum of $(CH_3)_3Ga$:NH_3 (frequency scale factor = 0.96), (b) experimental IR spectrum of $(CH_3)_3Ga$ + NH_3 at 50 Torr, and (c) $(CH_3)_3Ga$ + NH_3 at 300 Torr.

$(CH_3)_3Ga$:NH_3 adduct is shown in Figure 4a and is a good fit with the 50 Torr spectrum in Figure 4b. As with TMAl + NH_3, the disproportionately strong growth of some features is observed when the pressure is increased to 300 Torr, as seen by the marked peaks in Figure 4c. Thus, similar to TMAl + NH_3, we observe for TMGa + NH_3 the presence of a second, distinct product which increases in relative concentration as the pressure is increased. Following the same reasoning as that for TMAl + NH_3, this second product is assumed to involve the

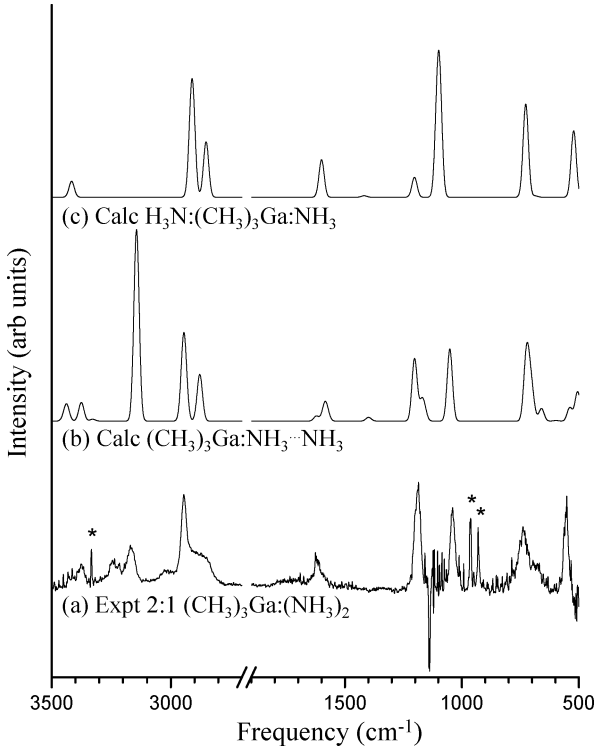

Figure 5. (a) Isolated experimental difference IR spectrum of 2:1 $(CH_3)_3Ga:(NH_3)_2$ and (b) calculated IR spectrum of hydrogen-bonded $(CH_3)_3Ga:NH_3\cdots NH_3$ (frequency scale factor = 0.96 for ν(N−H) and ν(C−H) modes, 0.95 all other modes), and (c) calculated IR spectrum of $H_3N:(CH_3)_3Ga:NH_3$ (frequency scale factor = 0.96). Asterisks represent residual NH_3 peaks.

bonding of a second NH_3 molecule to TMGa, i.e., a 2:1 $(CH_3)_3Ga:(NH_3)_2$ adduct.

As with TMAl + NH_3, we isolated the spectrum of the 2:1 $(CH_3)_3Ga:(NH_3)_2$ adduct via subtraction of a multiple (5.6) of the 50 Torr spectrum from the 300 Torr spectrum, the result of which is shown in Figure 5a. A negative peak at 1137 cm^{-1} and nearby artifacts are observed resulting from imperfect subtraction of the 1:1 $(CH_3)_3Ga:NH_3$ adduct, possibly due in part to peak shifting. The calculated spectrum of the 2:1 hydrogen-bonded $(CH_3)_3Ga:NH_3\cdots NH_3$ adduct is shown in Figure 5b, along with that of the 2:1 $H_3N:(CH_3)_3Ga:NH_3$ complex, shown in Figure 5c. Again, similar to the case with TMAl, the calculated hydrogen-bonded $(CH_3)_3Al:NH_3\cdots NH_3$ spectrum in Figure 5b predicts the major features of the experimental spectrum quite accurately. The calculated 2:1 $H_3N:(CH_3)_3Ga:NH_3$ spectrum represents a worse fit overall and notably fails to predict the strong peak at 3167 cm^{-1}. From this analysis, combined with the energetics calculations which predict that the hydrogen-bonded $(CH_3)_3Ga:NH_3\cdots NH_3$ adduct is more stable than the $H_3N:(CH_3)_3Ga:NH_3$ complex by 6.4 kcal/mol, we can assign the higher pressure 2:1 adduct as the hydrogen-bonded $(CH_3)_3Ga:NH_3\cdots NH_3$ adduct. The observed experimental frequencies are listed in Table 3, along with selected mode assignments taken from the corresponding calculated hydrogen-bonded $(CH_3)_3Ga:NH_3\cdots NH_3$ frequencies.

Conclusions

We have investigated the formation of gas-phase adducts of trimethylaluminum and trimethylgallium with ammonia using room-temperature FTIR experiments and DFT calculations. Our results indicate that at higher pressures, for both TMAl and TMGa, a product distinct from the well-known and observed

TABLE 3: Experimental and Selected Calculated Frequencies (cm^{-1}) and Relative Intensities (arb units) for the Hydrogen-Bonded $(CH_3)_3Ga:N^{(1)}H_3\cdots N^{(2)}H_3$ Adduct

exp	calc	I	assignment
	280	51	ν(Ga−N)
	311	24	$\delta(N^{(1)}H_3)_{rock} + \delta(N^{(2)}H_3)_{rock}$
	343	25	$\delta(N^{(1)}H_3)_{rock} + \delta(N^{(2)}H_3)_{rock}$
	471	4	ν_s(Ga−C_3)
	503	34	ν_{as}(Ga−C_3)
	507	37	ν_{as}(Ga−C_3))
552	539	32	$\delta(N^{(1)}H_3)_{rock} + \delta(CH_3)_{rock}$
	720	68	$\delta(CH_3)_{rock}$
739	726	97	$\delta(N^{(1)}H_3)_{rock} + \delta(CH_3)_{rock}$
1040	1051	169	$\delta_s(N^{(2)}H_3)$ umbrella
	1161	25	$\delta_s(CH_3)$
	1171	23	$\delta_s(CH_3)$
1186	1202	146	$\delta_s(N^{(1)}H_3)$ umbrella
1619	1622	12	$\delta_{as}(N^{(1)}H_3)$
2860	2876	51	$\nu(CH_3)$
	2880	52	$\nu(CH_3)$
2945	2945	43	$\nu(CH_3)$
3167	3143	449	$\nu_s(N^{(1)}H_3)$
	3328	4	$\nu_s(N^{(2)}H_3)$
	3375	44	$\nu_{as}(N^{(1)}H_3)$
	3437	19	$\nu_{as}(N^{(2)}H_3)$

[a] ν(C−H) and ν(N−H) modes scaled by 0.96; all other modes scaled by 0.95.

$(CH_3)_3M:NH_3$ adduct grows in. Comparison of the experimental and calculated IR spectra, along with calculations of the energetics, indicates that this second product is the result of hydrogen bonding of a second NH_3 molecule to the $(CH_3)_3M:NH_3$ adduct, which can be written as $(CH_3)_3M:NH_3\cdots NH_3$. Although we have not investigated the reaction of TMIn + NH_3 here, we suspect that the hydrogen-bonded $(CH_3)_3In:NH_3\cdots NH_3$ adduct may be observed for that system as well, based on the similar chemistries of TMAl, TMGa, and TMIn with NH_3. Because our experimental parameters fall within the typical range for MOCVD AlGaInN deposition, the formation of the hydrogen-bonded $(CH_3)_3M:NH_3\cdots NH_3$ adduct can be expected in MOCVD AlGaInN systems, particularly those operated at higher pressures. These results show that hydrogen bonding plays an important role in the interaction of ammonia with metalorganic precursors involving Al, Ga, and In and may also play a role in higher temperature parasitic chemical reactions during AlGaInN growth. The results also suggest that hydrogen bonding may be possible in systems involving TMAl, TMGa, and TMIn with PH_3 and AsH_3, which are relevant to AlGaInAs and AlGaInP growth. However, the substantially weaker ability of PH_3 and AsH_3 to form hydrogen bonds in comparison to NH_3[40] suggests that formation of the analogous 2:1 hydrogen-bonded adduct in these systems may be much less favorable.

Acknowledgment. Sandia is a multiprogram laboratory operated by Sandia Corp., a Lockheed Martin Co., for the United States Department of Energy's National Nuclear Security Administration under Contract No. DE-AC04-94AL85000. We especially acknowledge support from the Office of Basic Energy Sciences.

References and Notes

(1) Han, J.; Figiel, J. J.; Crawford, M. H.; Banas, M. A.; Bartram, M. E.; Biefeld, R. M.; Song, Y. K.; Nurmikko, A. V. *J. Cryst. Growth* **1998**, *195*, 291.

(2) Chen, C. H.; Liu, H.; Steigerwald, D.; Imler, W.; Kuo, C. P.; Craford, M. G.; Ludowise, M.; Lester, S.; Amano, J. *J. Electron. Mater.* **1996**, *25*, 1004.

(3) Sayyah, K.; Chung, B. C.; Gershenzon, M. *J. Cryst. Growth* **1986**, *77*, 424.

(4) Nakamura, F.; Hashimoto, S.; Hara, M.; Imanaga, S.; Ikeda, M.; Kawai, H. *J. Cryst. Growth* **1998**, *195*, 280.
(5) Safvi, S. A.; Redwing, J. M.; Tischler, M. A.; Kuech, T. F. *J. Electrochem. Soc.* **1997**, *144*, 1789.
(6) Mihopoulos, T. G.; Gupta, V.; Jensen, K. F. *J. Cryst. Growth* **1998**, *195*, 733.
(7) Thon, A.; Kuech, T. F. *Appl. Phys. Lett.* **1996**, *69*, 55.
(8) Creighton, J. R.; Breiland, W. G.; Coltrin, M. E. *Electrochem. Soc. Series 2002*, 28.
(9) Matsumoto, K.; Tachibana, A. *J. Cryst. Growth* **2004**, *272*, 360.
(10) Watari, F.; Shimizu, S.; Aida, K.; Takayama, E. *Bull. Chem. Soc. Jpn.* **1978**, *51*, 1602.
(11) Ault, B. S. *J. Phys. Chem.* **1992**, *96*, 7908.
(12) Müller, J.; Ruschewitz, U.; Indris, O.; Hartwig, H.; Stahl, W. *J. Am. Chem. Soc.* **1999**, *121*, 4647.
(13) Sywe, B. S.; Schlup, J. R.; Edgar, J. H. *Chem. Mater.* **1991**, *3*, 737.
(14) Almond, M. J.; Jenkins, C. E.; Rice, D. A.; Hagen, K. *J. Organomet. Chem.* **1992**, *439*, 251.
(15) Kim, S. H.; Kim, H. S.; Hwang, J. S.; Choi, J. G.; Chong, P. J.; Sywe, B. S.; Schlup, J. R.; Edgar, J. H.; Piocos, E. A.; Ault, B. S.; Bertolet, D. C.; Rogers, J. W.; Mazzarese, D.; Jones, K. A.; Conner, W. C. *Chem. Mater.* **1994**, 278.
(16) Durig, J. R.; Bradley, C. B.; Odom, J. D. *Inorg. Chem.* **1982**, *21*, 1466.
(17) Piocos, E. A.; Ault, B. S. *J. Mol. Struct.* **1999**, *476*, 283.
(18) Müller, J. *J. Am. Chem. Soc.* **1996**, *118*, 6370.
(19) Nakamura, K.; Makino, O.; Tachibana, A.; Matsumoto, K. *J. Organomet. Chem.* **2000**, *611*, 514.
(20) Makino, O.; Nakamura, K.; Tachibana, A.; Tokunaga, H.; Akutsu, N.; Matsumoto, K. *Appl. Surf. Sci.* **2000**, *159/160*, 374.
(21) Simka, H.; Willis, B. G.; Lengyel, I.; Jensen, K. F. *Progress in Crystal Growth and Characterization of Materials 7th European Workshop on MOVPE (EWMOVPE)*, June 8−11, 1997; Haus Wissenshcaft & Kultur: BERLIN, Germany, 1997; Vol. 35, p 117.
(22) Timoshkin, A. Y.; Bettinger, H. F.; Schaefer, H. F. *J. Phys. Chem. A* **2001**, *105*, 3240.
(23) Ikenaga, M.; Nakamura, K.; Tachibana, A.; Matsumoto, K. *J. Cryst. Growth* **2002**, *237*, 936.
(24) Watwe, R. M.; Dumesic, J. A.; Kuech, T. F. *J. Cryst. Growth* **2000**, *221*, 751.
(25) Creighton, J. R.; Breiland, W. G.; Coltrin, M. E.; Pawlowski, R. P. *Appl. Phys. Lett.* **2002**, *81*, 2626.
(26) Creighton, J. R.; Wang, G. T.; Breiland, W. G.; Coltrin, M. E. *J. Cryst. Growth* **2004**, *261*, 204.
(27) Becke, A. D. *J. Chem. Phys.* **1993**, *98*, 5648.
(28) Frisch, M. J.; Trucks, G. W.; Schlegel, H. B.; Scuseria, G. E.; Robb, M. A.; Cheeseman, J. R.; Montgomery, J. A., Jr.; Vreven, T.; Kudin, K. N.; Burant, J. C.; Millam, J. M.; Iyengar, S. S.; Tomasi, J.; Barone, V.; Mennucci, B.; Cossi, M.; Scalmani, G.; Rega, N.; Petersson, G. A.; Nakatsuji, H.; Hada, M.; Ehara, M.; Toyota, K.; Fukuda, R.; Hasegawa, J.; Ishida, M.; Nakajima, T.; Honda, Y.; Kitao, O.; Nakai, H.; Klene, M.; Li, X.; Knox, J. E.; Hratchian, H. P.; Cross, J. B.; Adamo, C.; Jaramillo, J.; Gomperts, R.; Stratmann,, R. E.; Yazyev, O.; Austin, A. J.; Cammi, R.; Pomelli, C.; Ochterski, J. W.; Ayala, P. Y.; Morokuma, K.; Voth, G. A.; Salvador, P.; Dannenberg, J. J.; Zakrzewski, V. G.; Dapprich, S.; Daniels, A. D.; Strain, M. C.; Farkas, O.; Malick, D. K.; Rabuck, A. D.; Raghavachari, K.; Foresman, J. B.; Ortiz, J. V.; Cui, Q.; Baboul, A. G.; Clifford, S.; Cioslowski, J.; Stefanov, B. B.; Liu, G.; Liashenko, A.; Piskorz, P.; Komaromi, I.; Martin, R. L.; Fox, D. J.; Keith, T.; Al-Laham, M. A.; Peng, C. Y.; Nanayakkara, A.; Challacombe, M.; Gill, P. M. W.; Johnson, B.; Chen, W.; Wong, M. W.; Gonzalez, C.; Pople, J. A. *Gaussian 03*, Revision A.5 ed.; Gaussian, Inc.: Pittsburgh, PA, 2003.
(29) Scott, A. P.; Radom, L. *J. Phys. Chem.* **1996**, *100*, 16502.
(30) Creighton, J. R. *J. Electron. Mater.* **2002**, *31*, 1337.
(31) Using TMAl vapor pressure curve from: Stringfellow, G. B. *Organometallic Vapor-Phase Epitaxy*, 2nd ed.; Academic Press: San Diego, CA, 1999.
(32) Using TMGa vapor pressure curve from: Plass, C.; Heinecke, H.; Kayser, O.; Luth, H.; Balk, P. *J. Cryst. Growth* **1988**, *88*, 455.
(33) Pelekh, A.; Carr, R. W. *J. Phys. Chem. A* **2001**, *105*, 4697.
(34) Creighton, J. R.; Wang, G. T. *J. Phys. Chem. A* **2005**, *109*, 133.
(35) Wang, G. T.; Creighton, J. R. *J. Phys. Chem. A* **2004**, *108*, 4873.
(36) Abu-Awwad, F. M. *THEOCHEM* **2004**, *683*, 57.
(37) Altmann, J. A.; Govender, M. G.; Ford, T. A. *Mol. Phys.* **2005**, *103*, 949.
(38) Huang, N.; MacKerell, A. D. *J. Phys. Chem. A* **2002**, *106*, 7820.
(39) Boese, A. D.; Chandra, A.; Martin, J. M. L.; Marx, D. *J. Chem. Phys.* **2003**, *119*, 5965.
(40) Sennikov, P. G. *J. Phys. Chem.* **1994**, *98*, 4973.